# UC Irvine

**Title**

Discrete parametric band conversion in silicon for mid-infrared applications

**Permalink**

**Journal**

**ISSN**

**Authors**

Tien, En-Kuang
Huang, Yuewang
Gao, Shiming
et al.

**Publication Date**

**DOI**

**Copyright Information**

Peer reviewed

# Discrete parametric band conversion in silicon for mid-infrared applications

**En-Kuang Tien, Yuewang Huang, Shiming Gao, Qi Song, Feng Qian, Salih K. Kalyoncu, and Ozdal Boyraz***

*EECS Department, University of California, Irvine, CA 92697 USA*
*\*oboyraz@uci.edu*

**Abstract:** Silicon photonics has great potential for mid-wave-infrared applications. The dispersion of waveguide can be manipulated by waveguide dimension and cladding materials. Simulation shows that <3μm wide conversion can be achieved by tuning the pump wavelength.

©2010 Optical Society of America

**OCIS codes:** (230.7390)Waveguide, planar ; (190.3270) Kerr effect.

## References and links

1. O. Boyraz, and B. Jalali, "Demonstration of 11dB fiber-to-fiber gain in a silicon Raman amplifier," IEICE Electron. Express **1**(14), 429–434 (2004).
2. R. Claps, D. Dimitropoulos, V. Raghunathan, Y. Han, and B. Jalali, "Observation of stimulated Raman amplification in silicon waveguides," Opt. Express **11**(15), 1731–1739 (2003).
3. O. Boyraz, and B. Jalali, "Demonstration of a silicon Raman laser," Opt. Express **12**(21), 5269–5273 (2004).
4. H. S. Rong, A. S. Liu, R. Jones, O. Cohen, D. Hak, R. Nicolaescu, A. Fang, and M. Paniccia, "An all-silicon Raman laser," Nature **433**(7023), 292–294 (2005).
5. X. Z. Sang, E. K. Tien, N. S. Yuksek, F. Qian, Q. Song, and O. Boyraz, "Dual-wavelength mode-locked fiber laser with an intracavity silicon waveguide," IEEE Photon. Technol. Lett. **20**(13), 1184–1186 (2008).
6. M. A. Foster, A. C. Turner, J. E. Sharping, B. S. Schmidt, M. Lipson, and A. L. Gaeta, "Broad-band optical parametric gain on a silicon photonic chip," Nature **441**(7096), 960–963 (2006).
7. M. A. Foster, A. C. Turner, R. Salem, M. Lipson, and A. L. Gaeta, "Broad-band continuous-wave parametric wavelength conversion in silicon nanowaveguides," Opt. Express **15**(20), 12949–12958 (2007).
8. Q. Lin, T. J. Johnson, R. Perahia, C. P. Michael, and O. J. Painter, "A proposal for highly tunable optical parametric oscillation in silicon micro-resonators," Opt. Express **16**(14), 10596–10610 (2008).
9. R. M. Osgood, Jr.N. C. Panoiu, J. I. Dadap, X. Liu, X. Chen, I. W. Hsieh, E. Dulkeith, W. M. Green, and Y. A. Vlasov, "Engineering nonlinearities in nanoscale optical systems: physics and applications in dispersion-engineered silicon nanophotonic wires," Adv. Opt. Photon. **1**, 162–235 (2009).
10. X. Zhang, S. Gao, and S. He, "Optimal Design of a Silicon-on-Insulator Nanowire Waveguide for Broadband Wavelength Conversion," Progress in Electromagnetics Research-Pier **89**, 183–198 (2009).
11. S. Gao, X. Zhang, Z. Li, and S. He, "Polarization-Independent Wavelength Conversion Using an Angled-Polarization Pump in a Silicon Nanowire Waveguide," IEEE J. Sel. Top. Quantum Electron. **16,** 250–256.
12. B. Jalali, V. Raghtmathan, R. Shori, S. Fathpour, D. Dimitropoulos, and O. Stafsudd, "Prospects for silicon mid-IR Raman lasers," IEEE J. Sel. Top. Quantum Electron. **12**(6), 1618–1627 (2006).
13. X. Liu, R. M. Osgood, Y. A. Vlasov, and M. J. GreenWilliam, "Mid-infrared optical parametric amplifier using silicon nanophotonic waveguides," Nat Photon advance online publication(2010).
14. P. Werle, F. Slemr, K. Maurer, R. Kormann, R. Mucke, and B. Janker, "Near- and mid-infrared laser-optical sensors for gas analysis," Opt. Lasers Eng. **37**(2-3), 101–114 (2002).
15. F. Capasso, R. Paiella, R. Martini, R. Colombelli, C. Gmachl, T. L. Myers, M. S. Taubman, R. M. Williams, C. G. Bethea, K. Unterrainer, H. Y. Hwang, D. L. Sivco, A. Y. Cho, A. M. Sergent, H. C. Liu, and E. A. Whittaker, "Quantum cascade lasers: Ultrahigh-Speed operation, optical wireless communication, narrow linewidth, and far-infrared emission," IEEE J. Quantum Electron. **38**(6), 511–532 (2002).
16. S. D. Jackson, and T. A. King, "High-power diode-cladding-pumped Tm-doped silica fiber laser," Opt. Lett. **23**(18), 1462–1464 (1998).
17. S. D. Jackson, "Single-transverse-mode 2.5-W holmium-doped fluoride fiber laser operating at 2.86 microm," Opt. Lett. **29**(4), 334–336 (2004).
18. R. Allen, and L. Esterowitz, "Cw Diode Pumped 2.3-Mu-M Fiber Laser," Appl. Phys. Lett. **55**(8), 721–722 (1989).
19. S. Tokita, M. Murakami, S. Shimizu, M. Hashida, and S. Sakabe, "Liquid-cooled 24 W mid-infrared Er:ZBLAN fiber laser," Opt. Lett. **34**(20), 3062–3064 (2009).
20. V. Raghunathan, D. Borlaug, R. R. Rice, and B. Jalali, "Demonstration of a Mid-infrared silicon Raman amplifier," Opt. Express **15**(22), 14355–14362 (2007).
21. R. A. Soref, S. J. Emelett, and W. R. Buchwald, "Silicon waveguided components for the long-wave infrared region," J. Opt. A, Pure Appl. Opt. **8**(10), 840–848 (2006).

22. S. Zlatanovic, J. S. Park, S. Moro, J. M. C. Boggio, I. B. Divliansky, N. Alic, S. Mookherjea, and S. Radic, "Mid-infrared wavelength conversion in silicon waveguides using ultracompact telecom-band-derived pump source," Nat Photon advance online publication(2010).
23. P. Klocek, Handbook of Infrared Optical Materials (M. Dekker, New York, 1991), p. 611.
24. P. Yang, S. Stankovic, J. Crnjanski, E. Teo, D. Thomson, A. Bettiol, M. Breese, W. Headley, C. Giusca, G. Reed, and G. Mashanovich, "Silicon photonic waveguides for mid- and long-wave infrared region," J. Mater. Sci. Mater. Electron. **20**(S1), 159–163 (2009).
25. R. A. Soref, S. J. Emelett, and A. R. Buchwald, "Silicon waveguided components for the long-wave infrared region," J. Opt. A, Pure Appl. Opt. **8**(10), 840–848 (2006).
26. M. Dinu, "Dispersion of phonon-assisted nonresonant third-order nonlinearities," IEEE J. Quantum Electron. **39**(11), 1498–1503 (2003).
27. M. Dinu, F. Quochi, and H. Garcia, "Third-order nonlinearities in silicon at telecom wavelengths," Appl. Phys. Lett. **82**(18), 2954–2956 (2003).
28. H. Garcia, and R. Kalyanaraman, "Phonon-assisted two-photon absorption in the presence of a dc-field: the nonlinear Franz–Keldysh effect in indirect gap semiconductors," J. Phys. At. Mol. Opt. Phys. **39**(12), 2737–2746 (2006).
29. S. Pearl, N. Rotenberg, and H. M. van Driel, "Three photon absorption in silicon for 2300–3300 nm," Appl. Phys. Lett. **93**(13), 131102 (2008).
30. G. Agrawal, Nonlinear Fiber Optics, Fourth Edition (Academic Press, 2006).
31. R. Stolen, and J. Bjorkholm, "Parametric amplification and frequency conversion in optical fibers," IEEE J. Quantum Electron. **18**(7), 1062–1072 (1982).
32. J. Hansryd, P. A. Andrekson, M. Westlund, L. Jie, and P. O. Hedekvist, "Fiber-based optical parametric amplifiers and their applications," IEEE J. Sel. Top. Quant. Electron. **8**(3), 506–520 (2002).
33. T. Andersen, K. Hilligsøe, C. Nielsen, J. Thøgersen, K. Hansen, S. Keiding, and J. Larsen, "Continuous-wave wavelength conversion in a photonic crystal fiber with two zero-dispersion wavelengths," Opt. Express **12**(17), 4113–4122 (2004).
34. J. P. Commin, D. G. Revin, S. Y. Zhang, A. B. Krysa, and J. W. Cockburn, "High performance, high temperature λ≈3.7," Appl. Phys. Lett. **95**(11), 111113 (2009).
35. A. D. Bristow, N. Rotenberg, and H. M. van Driel, "Two-photon absorption and Kerr coefficients of silicon for 850–2200 nm," Appl. Phys. Lett. **90**(19), 191104 (2007).

# 1. Introduction

Silicon on insulator (SOI) technology offers an attractive platform for nonlinear photonic devices. With good optical confinement and large nonlinear coefficient, waveguide-based planar devices can be integrated with state of art integrated circuits. Recently, devices using nonlinearities of silicon, such as Raman amplifier [1, 2], Raman laser [3–5], parametric amplification, and wavelength convertors [6–11], have attracted significant attention. These novel devices have been demonstrated in silicon waveguides to assist optical signal processing at telecommunication band ($\lambda$~1.5μm). However, two-photon absorption (TPA) and free-carrier absorption have been the major impediments of efficiency in these devices.

Mid wave infrared (MWIR), defined as wavelengths from 2μm to 6μm, has great potential in silicon because crystalline silicon has a good transparency window for wavelengths from 1.2μm all the way to 6.6μm, and free-carrier absorption is being replaced by less efficient three-photon absorption processes at these wavelengths [12,13]. MWIR wavelengths have attracted a lot of attention on gas sensing, free space communication, and thermal imaging for both civil and military purposes due to the air transmission window from 2μm to 5μm. Up to date, light sources beyond 3μm are provided by quantum cascade lasers that are commercially available [14, 15]. Lasers from 2μm to 3μm are also accessible in holmium doped fibers (2.1μm and 2.9μm) [16, 17], thulium (1.8-2.3μm) [18] and erbium (2.7μm) [19]. Particular problems arise at these wavelengths due to limitations on detectors, and also limited modulation and amplification capabilities on lasers. Matured InGaAs receivers and detectors have limited detection wavelength up to 1.7μm (can be extended to 2.5μm with electronic cooling), and detectors for MWIR are usually bulky and required operating at cryogenic temperature. All optical signal processing devices and wavelength converters can greatly enhance the capabilities of sources and detectors at MWIR through bi directional wavelength conversion and linking the near-IR sources and detectors to the MWIR.

Recently, Raman amplification in bulk silicon [20], waveguide design [21], and optical oscillator [8] has been demonstrated at MWIR. However, silicon in the previous experiments is either bulk silicon or waveguides fabricated on SOI wafers where the insulator material, silicon dioxide ($SiO_2$), is opaque among most of the MWIR band [13, 22]. As shown in Fig. 1,

SiO$_2$ has an attenuation coefficient of 10-100dB/cm in MWIR wavelengths except for the 2.9 −3.5μm window [23]. Hence, alternative insulator materials or different waveguide structures have to be adopted for MWIR applications. Several possible solutions have been proposed such as free standing waveguide with air cladding and hollow core waveguides with Bragg reflector surroundings [24]. Alternatively, Soref *et al* also proposed that different substrates materials, such as silicon nitride or sapphire (Al$_2$O$_3$), can be used [25]. Since sapphire is transparent from visible to 5.5μm [23] and silicon on sapphire (SOS) wafer is commercially available, we choose sapphire as the substrate material.

In this paper, we investigate the dispersive and nonlinear properties of silicon waveguides which are suitable for MWIR applications. In particular, we provide mode analysis and analytical modeling of silicon rib waveguides with sapphire substrate and air claddings. We show that dispersion engineering in these waveguides facilitate modulational instability based frequency band conversion that can create phase and amplitude replica of MWIR signals at wavelengths as low as 1.5um. Here, we show that dispersion engineered SOS waveguides can provide −10dB conversion efficiencies between 2.8μm and 6.2μm and between 1.5μm and 4.5μm at pump intensities up to 1 GW/cm$^2$. Waveguides with multiple zero-dispersion wavelengths (ZDWL) provide phase matching for pump wavelengths at both anomalous and normal dispersions due to higher-order dispersion. Further optimization of the waveguide geometry may facilitate ultra broadband frequency conversion in silicon waveguides.
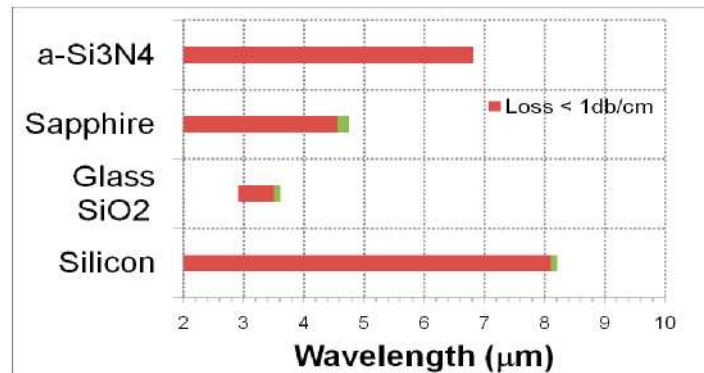


Fig. 1. 1dB/cm transmission spectrum of the materials for MWIR silicon devides.

## 2. Theoretical consideration

### 2.1 Kerr nonlinearity

Kerr effect is a third-order nonlinear effect, which induces intensity-dependent refractive index change. It contributes to various nonlinear effects, such as self-phase modulation, cross-phase modulation and four-wave mixing. At MWIR wavelengths, $n_2$ will scale down with the increasing wavelength of operation. Previously, detailed theoretical models have been presented by Garcia *et al*. to describe the dispersion of third-order nonlinearity including phonon assisted TPA and Kerr nonlinearity in silicon [26–28]. The nonlinear index change $n_2$ can be calculated from TPA coefficient via Kramer-Kronig relation. However, the theoretical predicted Kerr coefficient is underestimating n$_2$ measured experimentally in MWIR [29]. Since we have limited experimental data on n$_2$ measurements, a curve fitting of theoretical calculations is applied to available experimental measurements that give us a conservative estimate of n$_2$. Here we illustrate the scaling of n$_2$ with respect to the photon energy that is normalized by the bandgap energy of silicon (i.e. $h\nu/E_g$ where $E_g$ is the bandgap energy of silicon) in Fig. 2. Results indicate that $n_2$ scales down by factor of 2 from 2μm to 6μm.

## 2.2 Waveguide dispersion engineering

Bulk silicon has a normal dispersion value at wavelengths up to >8μm. On the other hand, cladding materials commonly used in silicon photonic devices have anomalous dispersion that can facilitate dispersion engineering at planar silicon devices. For instance, Fig. 3 illustrates the material dispersion of silicon with two common cladding materials: sapphire and $SiO_2$. Since sapphire also exhibits anomalous dispersion in MWIR region, sapphire cladding can be used to compensate silicon material dispersion. As a result, SOS bond well with low loss and low dispersion requirements for parametric devices envisioned at MWIR wavelengths.
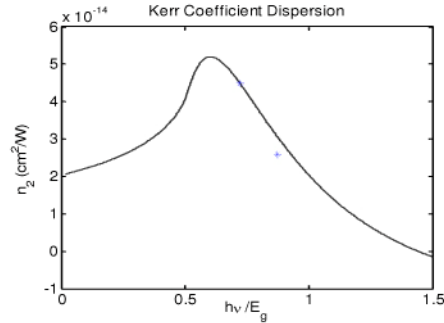


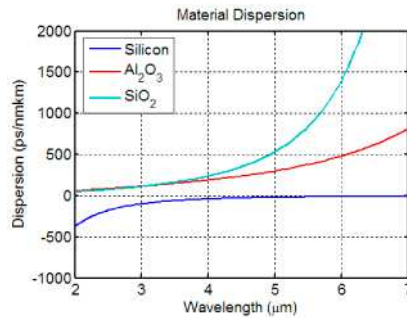Fig. 2. Predicted $n_2$ dispersion as a function of relative photon energy.



Fig. 3. Material dispersion of silicon, sapphire, and $SiO_2$.

To determine the performance of these parametric devices, we need to calculate the mode profiles of silicon waveguides at a given wavelength for a given geometry. Here, channel and rib waveguides are used and sapphire, $SiO_2$, and air are chosen to be the claddings materials, as illustrated in Fig. 4(a). We use finite element method (FEM) to solve the mode patterns at wavelengths from 1.1μm to 7μm. After the mode distribution is determined, the mode confinement factor, the effective waveguide index, and the modal area ($A_{eff}$) are calculated. For instance, Figs. 4(b) and 4(c) illustrate the mode profiles in a 1μm × 1μm rib waveguide with 500nm slab solved by FEM method at wavelengths of 2μm and 5μm, respectively. Figure 4(d) illustrates the size of the waveguides, which support 90% energy confinement in the silicon core, at various wavelengths. For instance, to confine 90% of energy in silicon core at 4μm, width and height of both channel and rib waveguides should be larger than 1.1μm. This confinement factor is particularly important to have effective interaction between pump and Stokes wave and to have large effective nonlinearity. The waveguides used in this paper are chosen to be around 1.1μm by 1.1μm to confine 90% energy for all the wavelengths launched into the waveguide. State of art silicon nanowires will not support good confinement at longer wavelengths and hence they are not suitable for long wavelength operations.
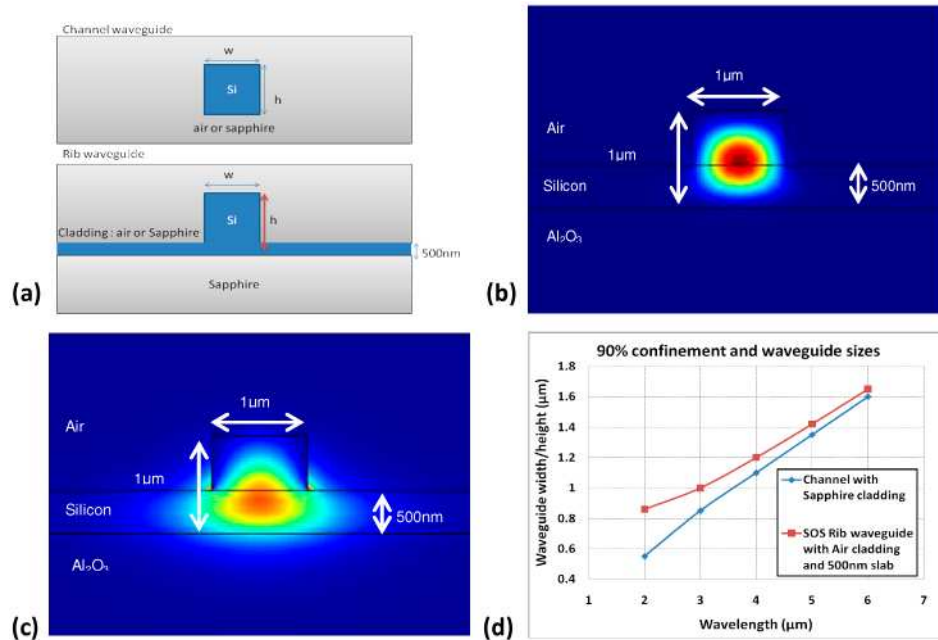
Fig. 4. (a) The proposed waveguide structure and the mode profiles of the rib waveguide at (b) 2μm and (c) 5μm. (d) Waveguide size that can support 90% confinement in silicon region at MWIR wavelengths.

The dispersion $D$ (or $\beta_2$) profile of the waveguides is calculated by using effective index $n_{eff}$ at various wavelengths:

$$D = -\frac{2\pi c}{\lambda^2}\beta_2(\omega) = \frac{\lambda}{c}\frac{d^2 n_{eff}(\lambda)}{d\lambda^2} \tag{1}$$

In particular, we are interested in the dispersion profile that can provide phase matching and facilitate frequency band conversion. The dispersion profiles of 1μm by 1μm channel waveguides with air, silica, and sapphire cladding are shown in Fig. 5(a). Here we obtain anomalous dispersion profile up to 5μm for all cladding materials but the dispersion profile is not suitable for phase matching. The dispersion of a 1μm by 1μm waveguide rib waveguide is estimated to be $D<200$ps/km/nm for wavelengths from 2μm to 6μm with both air and sapphire cladding, as shown in Fig. 5(b). These low dispersion values are particularly important and are suitable for broadband continuous wavelength conversion in the presence of high nonlinearity. Moreover, the dispersion can be "flattened" by changing the slab height in rib/ridge waveguides, as shown in Fig. 5(c). This is particularly important since a flat dispersion profile provides low phase mismatch within a longer wavelength span, which is favorable to achieve broadband wavelength conversion.

Further dispersion engineering can be achieved by scaling the waveguide dimensions. For instance, ZDWLs of the TE mode can be controlled from 2.8μm to 4.9μm in the rib waveguide on air cladding, Figs. 6(a) and (b), by increasing the cross sectional area from 0.8μm² to 1.6μm² with the same slab region. Also, the dispersion in these waveguides can be maintained within ~200ps/nm/km at wavelengths from 2μm to 5μm. The results indicate that, with similar waveguide geometry, the waveguide dispersion and hence the total dispersion of the silicon waveguide can be drastically changed to provide a means to control the ZDWL.
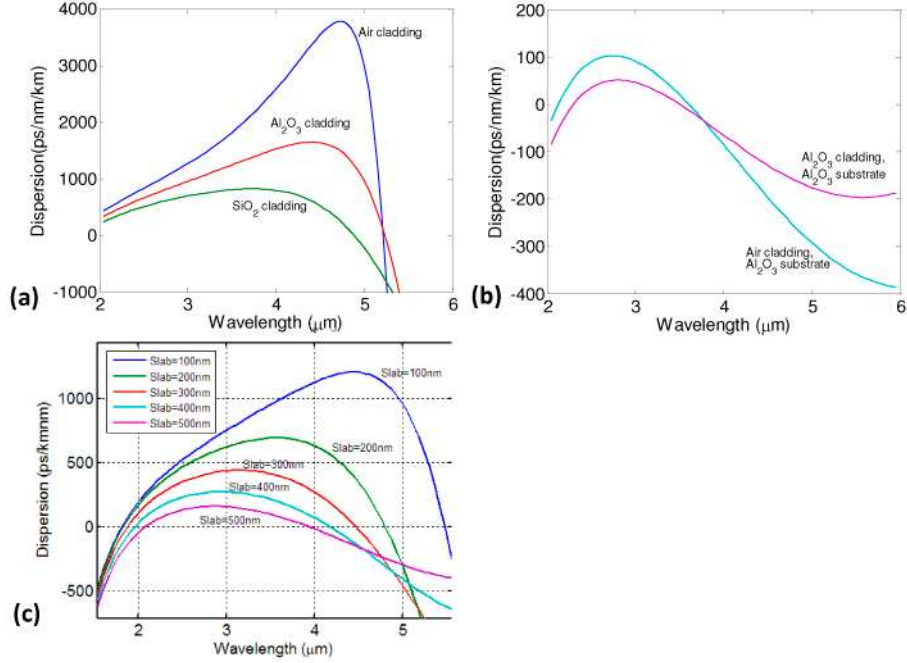
Fig. 5. (a) The calculated dispersion of channel waveguide with air, sapphire and SiO$_2$ as cladding materials. (b) Dispersion for rib/ridge waveguide with sapphire substrate and air and sapphire cladding. (c) Dispersion varies with the slab height of rib waveguide with sapphire substrate and air cladding.
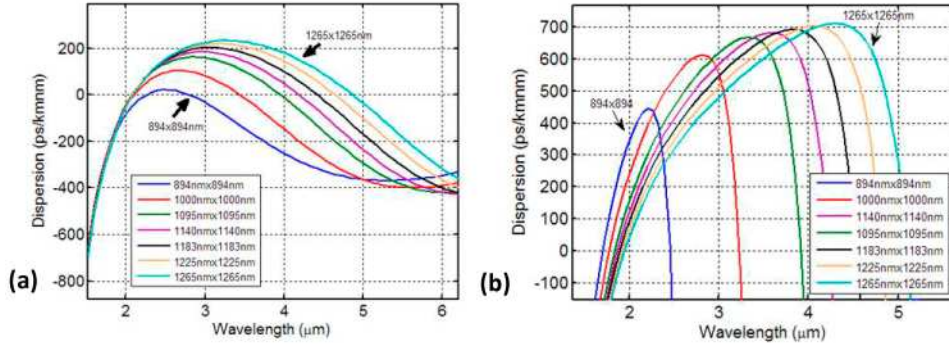


Fig. 6. Dispersions of the SOS rib waveguide with air cladding for (a) TE and (b) TM mode.

## 2.3 Four-wave-mixing at MWIR

The theory behind FWM process is well investigated. FWM process can be described by the following coupling equations [8, 30, 31]:

$$\frac{\partial A_p}{\partial z} = i\left(\gamma_p \left|A_p\right|^2 + 2\gamma_{pi}\left|A_i\right|^2 + 2\gamma_{ps}\left|A_s\right|^2\right)A_p + 2\gamma_{FWM}A_iA_sA_p^* \exp\left(i\Delta k_{Linear}z\right) \quad (2)$$

$$\frac{\partial A_i}{\partial z} = i\left(\gamma_i \left|A_i\right|^2 + 2\gamma_{is}\left|A_s\right|^2 + 2\gamma_{ip}\left|A_p\right|^2\right)A_i + \gamma_{FWM}A_p^2A_s^* \exp\left(-i\Delta k_{Linear}z\right) \quad (3)$$

$$\frac{\partial A_s}{\partial z} = i\left(\gamma_s \left|A_s\right|^2 + 2\gamma_{si}\left|A_i\right|^2 + 2\gamma_{sp}\left|A_p\right|^2\right)A_i + \gamma_{FWM}A_p^2A_i^* \exp\left(-i\Delta k_{Linear}z\right) \quad (4)$$

Here, subscripts $p,s,i$ represent pump, signal, and idler, parameters $A_p$, $A_s$ and $A_i$ represent the electric field amplitude of pump, signal and idler waves, respectively. The first term on the right represents the nonlinear term pertinent to the nonlinear phase modulations where self-phase modulation is caused by nonlinearity coefficient $\gamma_x$ ($x = p$, $s$, $i$) and cross-phase modulation is caused by the nonlinearity coefficient $\gamma_{xy}$ ($xy = ps$, $si$, $pi$). The second term in the equations represents four-wave mixing where $\gamma_{FWM}$ is the nonlinear coefficient involved with pump, signal, and idler. The nonlinearity coefficients, $\gamma$, is proportional to Kerr index $n_2$ and it is calculated as $\gamma = 2\pi n_2/\lambda A_{eff}$. Here, the nonlinear coefficient is determined by using the dispersion relationship mentioned in section 2.2. To obtain $\gamma_{xy}$, we use the Kerr coefficient at the averaged frequency, $\tilde{\omega}_{xy} = (\omega_x + \omega_y)/2$. For $\gamma_{FWM}$, Kerr coefficient at pump frequency is used. The effective area, $A_{eff}$, is calculated from the overlap integral of all the involved modes. The Eqs. (2)(3)(4) are usually solved using numerical method but a simple analytical expression can be obtained by assuming undepleted pump case where the parametric gain $g$ can be found as:

$$g = \left[ \left( \gamma_{FWM} P_{pump} \right)^2 - \left( \Delta k/2 \right)^2 \right]^{\frac{1}{2}} \tag{5}$$

Finally, the parametric gain can be found [32]:

$$G = \frac{P_s(L)}{P_s(0)} = 1 + \left[ \frac{\gamma_{FWM} P_{pump}}{g} \sinh(gL) \right]^2 \tag{6}$$

here $L$ is the interaction length. The parametric conversion efficiency $G_c$ can be written as

$$G_c = G - 1 \tag{7}$$

In order to achieve phase matching, the aggregate phase shifts $\Delta k$ due to linear and nonlinear effects should be minimized. $\Delta k$ can be written by dividing the source of the phase shift:

$$\Delta k = \Delta k_{linear} + \Delta k_{nonlinear} \tag{8}$$

here the difference in propagation constant ($\Delta k_{Linear}$) between pump, signal, and idler waves is calculated as: $\Delta k_{linear} = k_{signal} + k_{idler} - 2k_{pump}$, where $k_{pump}$, $k_{signal}$, $k_{idler}$ represent the propagation constants of pump, signal and idler waves, respectively. The nonlinear phase mismatch $\Delta k_{nonlinear} = 2(\gamma_{ip} + \gamma_{sp} - \gamma_{ip})P_{pump}$ are induced by the Kerr nonlinearity. And also from the conservation of energy $2\omega_{pump} = \omega_{signal} + \omega_{idler}$ is required. To achieve net gain, the total phase mismatch term $\Delta k$ should be reduced to zero and the nonlinear phase shift $\Delta k_{nonlinear}$ can be compensated by the negative wave vector mismatch $\Delta k_{linear}$ and the maximum parametric gain $g = \gamma P_{pump}$ is achieved. Conventionally, only second-order dispersion is considered in the analysis and higher-order dispersions are ignored. Under this assumption, the phase matching can be achieved at anomalous dispersion region. Since SOS waveguides exhibit a dispersion profile with multiple ZDWLs and large frequency range are considered, higher order dispersions also have significant contribution to the phase mismatch. Here, we simply use the total phase mismatch $\Delta k$ defined by Eq. (7).

The propagation constants of the SOS waveguides are calculated by solving the mode using finite-element method (COMSOL). By calculating the total phase mismatch in SOS waveguides, we found that the phase-matching condition $\Delta k = 0$ can be satisfied not only near the pump wavelength, but also at the discrete bands which are 2µm away from the pump wavelength. This behavior has been shown in photonic crystal fibers with similar dispersion profiles [33] and proposed in silicon waveguides at communication wavelengths [8, 9]. However, mode profiles of previous proposed silicon waveguides are not suitable for MWIR operations.

## 3. Wavelength conversion

Discrete and continuous wavelength conversion with silicon waveguide and sapphire cladding is demonstrated in dispersion optimized silicon waveguides. In conventional frequency conversion, phase matching is achieved in a continuous band of frequencies starting from pump, and hence the wavelength conversion is limited to signals at the vicinity of the pump wavelength. To achieve this goal, pump is usually placed near the zero dispersion wavelength of the waveguide. In the discrete band conversion, the pump is placed away from the zero dispersion wavelength to achieve phase matching between discrete set of frequencies far away from the pump wavelength. For instance, we use a 10mm long, $1.3\mu m^2$ ($1.14\mu m \times 1.14\mu m$) single mode silicon waveguides with 500nm slab height to support long wavelength operations and built on SOS with air cladding. Unlike conventional wavelength conversion, the nonlinear dispersion profile is being utilized by using a pump laser 700nm away from the ZDWLs, as shown in Fig. 7(a). The conversion efficiency in Fig. 7(a) is calculated using the formula presented by section 2.3. Here, the phase-matching condition, $\Delta k \cong 0$, is satisfied not only around the pump wavelength at $3.7\mu m$ but a discrete wavelength bands centered at $2.8\mu m$ and $6.2\mu m$, Fig. 7(a). The conversion band is estimated to be 15 nm at $6.2\mu m$ and the modulation instability and generate is $-8dB$, $-30dB$ and $-50dB$ conversion 1nm at $2.8\mu m$. Since the gain coefficient $g$ is a real number we also achieve efficiencies for pump intensity of $1GW/cm^2$, $0.1GW/cm^2$, and $0.01GW/cm^2$, respectively. We also show that using the same waveguide geometry with different pump wavelengths we can tune the center wavelength of the signal conversion band from $6\mu m$ to $4.5\mu m$, and center wavelength of idler conversion band from $2.5\mu m$ to $4\mu m$. Figure 7(b) illustrates the center wavelength of conversion band with respect to pump wavelengths varying from $3.6\mu m$ to $4.15\mu m$ with $1GW/cm^2$ pump power. It is clear that with this approach the phase matching to convert wavelengths separated by more than $3.5\mu m$ is feasible. In addition, $3.7\text{-}4.2\mu m$ wavelengths can be provided by quantum cascade lasers [34]. Additionally, using the low dispersion profile of SOS waveguide we can also achieve continuous band conversion at the vicinity of the pump laser.
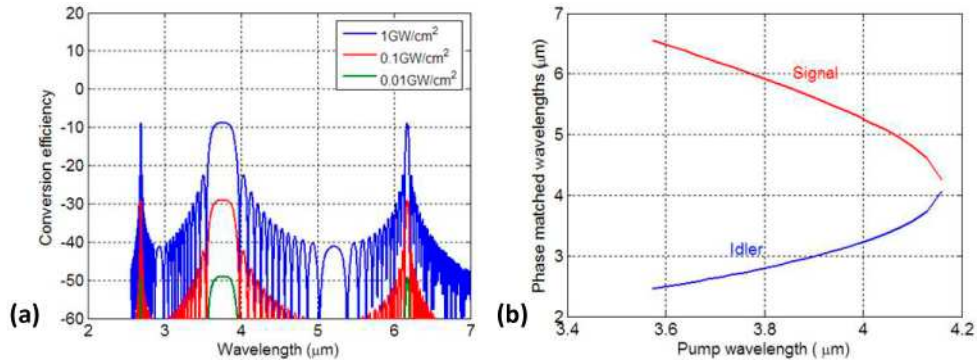


Fig. 7. (a)The conversion efficiency for $3.757\mu m$ pump wavelength which shows a discrete parametric conversion from $6.2\mu m$ to $2.8\mu m$. (b) Phase matching wavelengths ($\Delta k=0$) for various pump wavelengths.

In addition to conversion within mid-IR, wavelength conversion between MWIR and telecommunication wavelength has great potential for MWIR detection and free space communication applications. By scaling the waveguide dimension from $1.3\mu m^2$ to $1\mu m^2$, we find that the phase-matching condition can be satisfied between $1.5\mu m$ and wavelengths from $4\mu m$ to $>5\mu m$ in a 10mm long, $1\mu m$ by $1\mu m$ waveguide with 500nm slab height. The dispersion of the TE mode in such waveguide is shown in Fig. 6(a).

Figure 8(a) illustrates the calculated wavelength conversion profile for pump laser at $2.3\mu m$. We achieved discrete band conversion between $1.55\mu m$ and $5.1\mu m$. The conversion efficiencies of varies pump intensities are illustrated in Fig. 8(a). While the pump is at $2.35\mu m$, $-20dB$ conversion efficiency is achievable with $0.1\ GW/cm^2$ and. The conversion

efficiency increases to −3dB when the pump intensity is increase to 1GW/cm$^2$, as shown in Fig. 8(a). Here, the conversion bandwidth is estimated to be 20nm at 5.1μm and 2nm at 1.5μm. Similar to previous case, we can achieve discrete band conversion by using different pump wavelengths from 4μm to 5.2μm in 1μm$^2$ waveguide. For instance, Fig. 8(b) illustrates the center wavelengths of the discrete bands that satisfy the phase matching and provide wavelength conversion with respect to different pump wavelengths. The center wavelength of the signal band can be tuned from 1.48μm to 1.6μm and center wavelength of the idler band can be tuned from 4.2μm to 5.2μm, with pump wavelength changed from 2.18μm to 2.38μm and 1GW/cm$^2$ pump power. Note that since pump is below the half of the silicon bandgap, pump is free from degenerate TPA. However, non-degenerate TPA between signal and pump will show up as the dominant nonlinear loss mechanism. For instance, for pump intensities of 1GW/cm$^2$ the nondegenerate TPA [35] may introduce −2.5dB/cm loss for short wavelength signals. The wavelength conversion with pump wavelengths above 2.34μm will still provide conversion of mid-IR signals to short wavelengths that can be detected standard telecom detectors based of InGaAs. Three photon absorption (3PA) is also present in the system, but as a simple calculation using the measured 3PA coefficient from Ref [29] shows that the 3PA loss and FCA are negligible at these intensity levels.
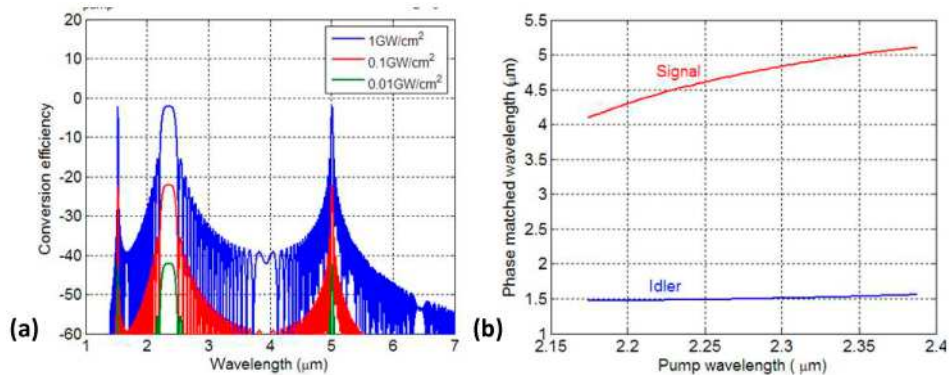


Fig. 8. (a) Conversion efficiency for 1GW/cm$^2$, 0.1GW/cm$^2$, and 0.01GW/cm$^2$ pump intensity at 2.4μm. The maximum conversion efficiency is 0dB, −20dB, and −40dB, respectively. (b) Phase matching condition ($\Delta k$=0) for 1μm rib waveguide.

## 4. Summary

Wavelength conversion in silicon has great potential for next generation optical communication and sensing applications at MWIR wavelengths. In particular, sapphire cladding can provide low loss waveguides suitable for operation at those wavelengths. Here we illustrate the prospect of these waveguides for parametric process at long wavelengths. We show that by manipulating the waveguide dimensions, the ZDWLs can be tuned from 4 μm to 5 μm. We estimate that >3μm discrete wide-band conversion in mid-IR achievable at 3.7μm pumping with ~-10dB conversion efficiency in a 1cm long waveguide with intensity at 1GW/cm$^2$. We also show that wavelength conversion from 4 to 5μm to telecommunication wavelengths are possible for high sensitivity detection and source generation at MWIR.

## Acknowledgement